HHS Public Access

Author manuscript

Am J Psychiatry. Author manuscript; available in PMC 2022 January 01.

Published in final edited form as:

Am J Psychiatry. 2021 January 01; 178(1): 48–64. doi:10.1176/appi.ajp.2020.19070698.

Antibodies from children with PANDAS bind specifically to striatal cholinergic interneurons and alter their activity

Jian Xu, Ph.D.[1], **Rong-Jian Liu, Ph.D.**[1], **Shaylyn Fahey, B.S.**[1], **Luciana Frick, Ph.D.**[1,2], **James Leckman, M.D., Ph.D.**[3,4], **Flora Vaccarino, M.D.**[3,5], **Ronald S. Duman, Ph.D.**[1], **Kyle Williams, M.D., Ph.D.**[1,6], **Susan Swedo, M.D.**[7,8], **Christopher Pittenger, M.D., Ph.D.**[1,3,9,*]

[1]Department of Psychiatry, Yale University School of Medicine, 34 Park Street, New Haven, CT 06519

[2]Current address: Hunter James Kelly Research Institute, University at Buffalo

[3]Child Study Center, Yale University School of Medicine

[4]Department of Pediatrics, Yale University School of Medicine

[5]Department of Neuroscience, Yale University School of Medicine

[6]Current address: Department of Psychiatry, Massachusetts General Hospital and Harvard Medical School

[7]Pediatrics and Developmental Neuroscience Branch, National Institute of Mental Health

[8]PANDAS Physicians Network

[9]Interdepartmental Neuroscience Program, Yale University

Abstract

Objective: Pediatric obsessive-compulsive disorder (OCD) sometimes appears rapidly, even overnight, often after an infection. Pediatric Autoimmune Neuropsychiatric Disorder Associated with Streptococcus, or PANDAS, describes such a situation after infection with *Streptococcus pyogenes*. PANDAS may result from induced autoimmunity against brain antigens, though this remains unproven. Pilot work suggests that IgG antibodies from children with PANDAS bind to cholinergic interneurons (CINs) in the striatum. CIN deficiency has been independently associated with tics in humans and with repetitive behavioral pathology in mice, making it a plausible locus of pathology.

[*]Address correspondence to: Christopher Pittenger, Yale University School of Medicine, 34 Park Street 333b, New Haven, CT 06519. Phone: 203-974-7675. christopher.pittenger@yale.edu.

Author Contributions

JX conducted immunohistochemistry, biochemistry, and image processing and performed data analysis, with support from SF; KW and SS provided serum samples; RJL performed electrophysiological experiments and analyzed electrophysiological data; FV provided human post-mortem tissue sections; RSD and LRF provided key intellectual contributions; CP supervised the study; JX and CP led manuscript writing; all authors contributed to data interpretation and manuscript preparation.

Disclosures

Dr. Pittenger has served as a consultant in the past year for Biohaven Pharmaceuticals, Teva Pharmaceuticals, and Brainsway Therapeutics and has performed research under contract with Biohaven and with Blackthorn Therapeutics, Ltd., on unrelated projects. All other authors report no competing interests. The authors have declared that no conflict of interest exists.

Methods: Binding of IgG to specific neurons in human and mouse brain slices was evaluated *ex vivo* after incubation with serum from 27 children with rigorously characterized PANDAS, both at baseline and after intravenous immunoglobulin (IVIG) treatment, and 23 matched controls. Binding was correlated with symptom measures. Neural activity after serum incubation was assessed in mouse slices using molecular markers and electrophysiological recording.

Results: IgG from children with PANDAS bound to CINs, but not to multiple other neuron types, more than IgG from controls, in three independent cohorts of patients. IVIG reduced IgG binding to CINs; this reduction correlated with symptom improvement. Baseline PANDAS sera decreased activity of striatal CINs, but not of parvalbumin-expressing GABAergic interneurons, and altered their electrophysiological responses, in acute mouse brain slices. Post-IVIG PANDAS sera and IgG-depleted baseline sera did not alter the activity of striatal CINs.

Conclusions: These findings provide strong evidence for striatal CINs as a critical cellular target that may contribute to pathophysiology in children with rapid-onset OCD symptoms, and perhaps in other conditions.

INTRODUCTION

Obsessive-compulsive disorder (OCD) occurs in 1% to 3% of children and adolescents in the United States, and a comparable proportion worldwide (1, 2). In a subset of pediatric OCD cases, onset of neuropsychiatric symptoms is strikingly abrupt; this has been termed pediatric acute-onset neuropsychiatric syndrome, or PANS (3, 4). In some, symptom onset is temporally associated with an infectious illness, often with group A beta-hemolytic streptococcus (GAS) (5). This natural history, and the presence of a constellation of characteristic associated symptoms (e.g. separation anxiety, severely restricted food intake, enuresis, choreiform movements, handwriting deterioration), suggests that this presentation may represent a discrete clinical entity, which has been termed *pediatric autoimmune neuropsychiatric disorders associated with streptococcal infection*, or PANDAS. The incidence and prevalence of PANDAS are unknown. PANDAS and PANS have been the focus of considerable research, and some controversy, over three decades (5–7).

It has been suggested that PANDAS results from the post-infectious production of antibodies that target the basal ganglia, perhaps through the phenomenon of molecular mimicry (8, 9). This hypothesis draws an analogy to Sydenham chorea (SC), a well characterized post-Streptococcal autoimmune neurological disorder in which comorbid OCD symptoms are often seen (5, 10–12). This pathophysiological hypothesis implies the presence of pathogenic anti-brain antibodies in children with PANDAS (13, 14). Indeed, autoantibodies against neuronal targets have been described in several studies, including against lysoganglioside (15), tubulin (16) and dopamine D1 and D2 receptors (17, 18). However, none of these binding patterns has been consistently replicated across studies. PANDAS sera have been shown *in vitro* to alter activation of calcium calmodulin protein kinase II (CaMKII) in a human neuroblastoma cell line and to reduce cyclic adenosine monophosphate (cAMP) in a mouse fibroblast cell line expressing human D2R (15, 18).

Immune modulatory treatments such as plasmapheresis and intravenous immunoglobulin (IVIG) have shown promise in some trials, though others have been inconclusive (19–22). Antibiotic prophylaxis has also been found to be effective in reducing the rate of recurrent episodes in some studies (23), though again, others have not found clear benefit (24, 25). In animal studies, immunization with GAS can produce abnormal behavior, and passive transfer of sera from these GAS-exposed rodents to naive animals can recapitulate some of these abnormalities (26, 27). Thus, convergent evidence from multiple studies supports the concept of immunologic pathogenesis in PANDAS, but non-replication has been common, and the literature has yet to converge on a clear understanding of the pathophysiology of the condition – or even if it is appropriately conceived as a discrete entity.

The pathophysiology of OCD and tic disorders is incompletely understood (28, 29). Substantial evidence implicates dysregulation of cortico-basal ganglia circuits in both conditions (30–35), as well as in PANDAS. The striatum, which consists in primates of the caudate and putamen, is the primary input nucleus of the basal ganglia and integrates synaptic inputs from limbic and cortical regions (36). The vast majority of neurons in the striatum (~95% in rodents) consists of GABAergic medium spiny neurons (MSNs). Only a small fraction (~5%) are interneurons (37), of which GABAergic interneurons are the most abundant. They can be classified based on their expression of markers such as parvalbumin (PV), somatostatin (SOM), neuropeptide Y (NPY), and neuronal nitric oxide synthase (nNOS). A distinct, small population of large, tonically active cholinergic interneurons (CINs) is characterized by expression of choline acetyltransferase (ChAT). Although few in number, these interneurons are key regulators of striatal function (38–41). Both CINs and PV-expressing GABAergic interneurons are reduced in number in the caudate and putamen of Tourette syndrome (TS) individuals (42–44). Transcriptomic analysis of post-mortem striatum from TS similarly reveals reduced expression of interneuron-associated genes (43). Experimental depletion of these cells in developmentally normal mice produces repetitive behavioral pathology (45, 46), suggesting that this deficit is causally related to symptomatology.

In a small pilot study (N=5), we found that IgG antibodies from children with rigorously characterized PANDAS showed significantly higher *in vivo* binding to CINs in mouse than IgG from age- and gender-matched healthy controls. This elevated IgG binding to CINs resolved in parallel with symptom improvement in serum collected after IVIG treatment (47). This suggests that binding of IgG to striatal CINs may contribute to pathophysiology in PANDAS.

Here, we confirm elevated IgG binding to CINs, but not to other striatal neurons, both in the original 5 PANDAS patients and in two additional independent cohorts of patients, and in both mouse and human striatal tissue. Reduced IgG binding to CINs correlated with symptom improvement after the IVIG treatment (21, 47). Furthermore, PANDAS serum reduces molecular markers of spontaneous activity of CINs, but not of PV-expressing interneurons, in an *ex vivo* assay, and reduces the electrophysiological response of CINs to the glutamate agonist α-amino-3-hydroxy-5-methyl-4-isoxazolepropionic acid (AMPA), compared to matched control serum. Post-IVIG sera and IgG-depleted baseline sera did not alter activity of CINs, suggesting that serum IgG is necessary for the cellular effects. These

data reveal a novel mechanism whereby specific antibodies in children with PANDAS can bind to and inhibit CINs, which may contribute to symptomatology.

METHODS

PANDAS serum

These investigations of human serum samples were approved by the Human Investigations Committees of Yale University and the NIMH. Parents gave written informed consent to participate in the study, and children gave assent. In the first two cohorts of patients analyzed, sera from 11 children with a well-substantiated diagnosis of PANDAS were selected from a clinical trial performed at the National Institute of Mental Health (NIMH) and Yale University (NCT01281969), as described previously (21). Subjects met rigorous clinical and laboratory criteria for a diagnosis of PANDAS (5) and were additionally selected for having a robust clinical response to treatment with intravenous immunoglobulin (IVIG) (21); we reasoned that IVIG responders are most likely to have antibody-mediated pathology. The Children's Yale-Brown Obsessive Compulsive Scale (CY-BOCS) (48) was assessed at baseline (before IVIG treatment) and at 6, 12, and 18 weeks; serum from baseline and 12-week visits (visits 1 and 3 in the clinical trial; see Figure S1) were used in the current study. Mean CY-BOCS scores were 28.64±1.03 SEM at baseline and 5.64±1.59 SEM at 3 months, after 1 or 2 rounds of IVIG treatment. A third cohort of 16 PANDAS subjects and 13 matched controls was obtained from the same NIMH PANDAS clinic; these samples were drawn from several different studies and were not pre-selected for IVIG response. Age- and gender-matched healthy subjects with no clinically significant OCD or tic symptoms were collected and stored by the same investigators at the NIMH (SS and her team) and were stored and tested in parallel. The first patient cohort, consisting of 5 PANDAS subjects and 5 matched controls, has been described previously (47). All samples were aliquoted into small volume upon arrival at Yale and stored at −80 °C until use. Demographic data for all subjects are listed in Table S1 and S2. All sera were anonymized before being sent from the NIMH to Yale for analysis; all analyses were performed blind to diagnosis and condition.

Normal human brain tissue

The collection and preparation of formalin-fixed normal human brain tissue have been described previously (43). 50 μm coronal sections of caudate and putamen (2 sections per serum) were used for serum antibody binding and immunostaining, as further detailed below.

Animals

All experimental procedures were approved by the Yale University Institutional Animal Care and Use Committee, in accordance with the NIH Guide for the Care and Use of Laboratory Animals. Male and female C57BL/6J mice were purchased from the Jackson Laboratory (Bar Harbor, Maine, http://jaxmice.jax.org/strain/013636.html). Double-transgenic D1-DARPP-32-FLAG/ D2-DARPP-32-Myc were backcrossed to C57BL/6J for at least 9 generations and have been described previously; the transgenically expressed FLAG and Myc epitope tags allow dissociable immunostaining of D1- and D2-expressing

MSN populations (49, 50). All mice were maintained on a 12 h light/dark cycle and used at 3–6 months of age.

Reagents and antibodies

N-methyl-D-glucamine (NMDG), glucose, thiourea, sodium pyruvate, sodium ascorbate, tetrodotoxin (TTX), Sudan Black B, Triton X-100 were obtained from Sigma (St. Louis, MO). DA and other chemicals used for electrophysiology (Figure S12) were also obtained from Sigma, with the exception of 5-HT and AMPA, which were obtained from Tocris (Ellisville, MO). Paraformaldehyde (PFA), KCl, and other chemicals used for acute brain slice analysis (Figures 3 and 5) were obtained from JT Baker (Phillipsburg, NJ). Ketamine (Ketaset) was obtained from Zoetis (Madison, NJ). Xylazine (Anased) was obtained from Akorn, Inc. (Decatur, IL). Antibodies used in immunohistochemical staining are listed in Table S3.

Determination of serum IgG titer; IgG depletion

Total IgG titers in control and PANDAS sera were determined using IgG (Total) Human ELISA Kit (Thermo Scientific, Rockland, IL) following manufacturer's instructions. Pre-diluted sera were added to microplates pre-coated with an anti-human IgG capture antibody and incubated for 2 h at room temperature (RT). After washes, a HRP-conjugated anti-human IgG detection antibody was added for 1 h at RT. After extensive washes, 3,3',5,5'-tetramethylbenzidine (TMB) solution was added to each well for 15 min. The reaction was stopped with 1 M phosphoric acid and optical density reading was obtained using an MQX200 μQuant plate reader (Bio-tek, Winooski, VT) at 450 nm. Human IgG standard provided in the kit was used as a reference to determine IgG concentration in each serum. All sera were diluted in 1×PBS + 0.1% bovine serum albumin to 500 mg/dL IgG and anonymized before testing.

For IgG depletion, baseline (pre-IVIG treatment) PANDAS sera of 11 subjects (Table S1) were incubated with Protein A/G agarose beads (Thermo Scientific) for 2 h at 4 °C. Supernatants were collected by brief centrifugation (1000×g for 1 min). Supernatants were mixed with fresh Protein A/G agarose beads for a second round depletion. To confirm IgG depletion, small aliquots from both batches of supernatants were tested on dot blot using a rabbit anti-human IgG antibody (Abcam, Cambridge, MA) and HRP-conjugated goat anti-rabbit secondary antibody (Thermo Scientific). Membranes were developed using Chemiluminescent Substrate kit (Thermo Scientific) and visualized on a ChemiDoc XRS+ system (Bio-Rad, Hercules, CA).

Immunohistochemistry

For Figures 1 and 4, mice were anesthetized by intraperitoneal injection of ketamine (100 mg/kg) with xylazine (10 mg/kg) and transcardially perfused with cold 4% paraformaldehyde in 1×PBS (pH 7.4). Brains were fixed overnight in 4% PFA at 4 °C, followed by equilibration in 30% sucrose for 48 h at 4°C. Striatal slices were cut at 20 μm using a Leica CM3050S cryostat (Leica, Buffalo Grove, IL). Slices were stored in a cryoprotectant solution (30% glycerin, 30% ethylene glycol in 1×PBS pH 7.4) at −20 °C until use. All staining was done using WT C57BL6 mice, expect for examination of D1R-

and D2R-expressing MSNs, for which we used D1-FLAG/D2-Myc double transgenic mice (49, 50).

Brain sections were washed 3×10 min in 1×PBS (pH 7.4) to remove cryoprotectant, followed by incubation in freshly prepared 0.1% Sudan Black (in 70% ethanol) for 10 min at RT to reduce autofluorescence. Slices were washed 3×10 min in 70% ethanol and 3×10 min in 1×PBS. Slices were blocked in 1×PBS + 0.3% Triton X-100 supplemented with 5% donkey serum (Jackson Immunoresearch, West Grove, PA) for 1h at RT, and then incubated overnight at 4°C with PANDAS or healthy control serum at 1.25 mg/dL (diluted in blocking buffer; this dilution was found in extensive pilot experiments to provide optimal signal-to-noise for cell body staining). For staining with mouse primary antibodies (anti-PV, anti-nNOS, and anti-FLAG), slices were additionally blocked in Mouse-on-Mouse (MOM) reagent (Vector Laboratories, Burlingame, CA), following the manufacturer's instructions. Slices were then washed 3×10 min in 1×PBS + 0.3% Triton X-100 and incubated with primary antibodies (see Table S3) in blocking buffer overnight at 4 °C. Sections were double-immmunostained with anti-human IgG to identify serum IgG binding (green) and selected neuronal markers (ChAT, PV, nNOS, and antibodies to the epitope tags FLAG and Myc to detect MSNs in D1-DARPP-32-FLAG/ D2-DARPP-32-Myc; red). The next day, slices were washed 3×10 min in 1×PBS + 0.3% Triton X-100, and then incubated with fluorophore-conjugated secondary antibodies (see Table S3) for 1 h at RT. After 3×10 min washes in 1×PBS, slices were mounted in Vectashield HardSet Mounting Medium (Vector Laboratories), coverslipped, and stored at 4 °C.

For illustrative purposes, IgG binding was visualized by sequential scanning of slices on an Olympus Fluoview FV-1000 confocal microscope with a 40×/1.30NA objective (Olympus, Japan, Figures 1A, 3A, 3F, and 4A, and corresponding high-magnification panels in Supplementary Figures).

For quantification, we used lower-magnification images collected using single-photon fluorescence imaging; these images are of lower resolution than confocal images and do not resolve the z-dimension as well, but they allow us to quantify an order of magnitude more cells (see Figures S2 and S16–S19). Single-photon fluorescence images were collected using an Axioskop 2 fluorescent microscope with a 20×/0.8 NA objective (Zeiss, Germany) or an Axio Scope A1 fluorescent microscope with a 10×/0.45 NA objective (Zeiss). 36–48 images from 4–6 mice were taken per serum in the dorsal striatum; 12–16 images from 4–6 mice were taken for each serum in the medial septum. Microscope settings were kept constant (2500 ms- 3500 ms exposure for IgG imges, 1000 ms-1500 ms for neuronal markers: ChAT, PV, nNOS, FLAG and Myc) across all images between which comparisons were made. In some cases (Figures 1 and S6), due to limited microscope availability, images were captured using different microscopes for different cohorts. To compensate for differences in background binding, data were normalized to the mean value of the control samples processed in the same batch. Microscope fields were chosen randomly without overlap within dorsal striatum, using lateral ventricle as an anatomical landmark, to ensure that comparable fields were examined for all sera; the distribution of images and the total number of cells of each type quantified is shown in Figure S2. Cells counts did not differ between PANDAS and control groups for any neuron type.

Human brain sections were triple-immunostained with anti-human IgG and selected neuronal markers (ChAT and PV) following the same protocol. 3-color images were collected using an Olympus Fluoview FV-1000 confocal microscope with a 40×/1.30NA objective. Triple-staining and confocal imaging limit the number of cells quantified but were used for this experiment to conserve human tissue samples.

Acute brain slice preparation, *ex vivo* serum treatment, and quantification of phospho-rpS6

For the functional assay shown in Figures 3 and 5, acute brain slices were prepared from male and female wild-type mice and treated *ex vivo* with PANDAS (pre-IVIG, post-IVIG and IgG-depleted pre-IVIG) or control serum. Mice were sacrificed by cervical dislocation; brains were quickly removed and placed in ice-cold oxygenated NMDG-based aCSF (artificial cerebrospinal fluid), as previously described (51). 100 μm coronal slices through the striatum (see Figure S2) were cut using a Leica VT1000S vibratome (Leica Microsystems, Bannockburn, IL, USA) in the NMDG solution containing (in mM): 92 NMDG, 2.5 KCl, 1.25 NaH_2PO_4, 30 $NaHCO_3$, 20 HEPES, 10 $MgSO_4$, 0.5 $CaCl_2$, 25 glucose, 2 thiourea, 3 sodium pyruvate and 5 sodium ascorbate, pH 7.35, saturated with 95% O_2/5% CO_2.

Slices were recovered in NMDG-aCSF for 10 min at 32°C before being transferred to regular aCSF containing (in mM): 119 NaCl, 2.5 KCl, 1.25 NaH_2PO_4, 24 $NaHCO_3$, 2 $CaCl_2$, 2 $MgSO_4$ and 12.5 glucose for 1 h at 30 °C under constant oxygenation with 95% O_2/5% CO_2. After recovery, slices were treated with control drugs (TTX 1 μM; KCl 20 mM, 0.1% DMSO in aCSF), control serum (1.25 or 6.25 mg/dL), or PANDAS serum (baseline, post-IVIG, or IgG-depleted baseline; 1.25 or 6.25 mg/dL) for 1 h at 30°C. A subset of slices was treated with aCSF with 0.1% DMSO in each experiment; data from other conditions was normalized to this vehicle condition for analysis. After treatment, slices were fixed in cold 4% paraformaldehyde (PFA) in 1×PBS (pH 7.4) containing 5 mM NaF for 1 h at 4 °C.

Sections shown in Figure 3 were double-immunostained for phospho-rpS6 (green) and ChAT (red) or PV (red), as described above. For ChAT/P-rpS6 staining, 23–56 images from 4–7 mice were taken in the dorsal striatum for each serum and 100–350 CINs were quantified for each serum. For PV/P-rpS6 staining, 40–52 images from 5 mice were taken in the dorsal striatum and 60–100 PV^+ interneurons were quantified for each serum. Total cells counted did not differ between PANDAS and control groups. Sections shown in Figure 5 were triple-immunostained with anti-human IgG, anti-ChAT, and anti-PV, as described above. Images were collected using an Olympus Fluoview FV-1000 confocal microscope with a 40×/1.30NA objective. Triple-immunostaining and confocal imaging limit the number of cells quantified but were used for this experiment to conserve serum.

Image processing and quantification

Automated quantitation of mean fluorescence intensity within each cell was achieved using Fiji ImageJ from NIH (https://imagej.net/Fiji/Downloads) with batch processing, as illustrated in Figure S3. Neuronal marker immunostaining (ChAT, PV, N-NOS, FLAG, or c-Myc) was thresholded and used to generate regions of interest corresponding to cell

bodies of the selected cell type. The number and spatial extent of these cellular ROIs was quantified to ensure between-group comparability. The total ROIs per section obtained for each serum was interpreted as cell number for the selected cell type. This spatial filter was then overlayed on the corresponding anti-human IgG or phospho-rpS6 image, and immunostaining within each cellular ROI was quantified. Background IgG or phospho-rpS6 signal was subtracted to generate an adjusted value for each cell. This procedure is illustrated in Figure S3. Although this procedure is wholly automated, serum identity was anonymized until all the values were retrieved, as an additional safeguard for the rigor of the analysis.

Brain slice electrophysiology

Brain slices were prepared as previously described (52). Briefly, mice were anesthetized using chloral hydrate (400 mg/kg, i.p.) and brains removed and placed in ice-cold artificial cerebrospinal fluid (ACSF) in which sucrose (252 mM) was substituted for NaCl (sucrose-ACSF). A block of tissue containing corticostriatal and coronal slices (400 μm) were cut in sucrose-ACSF with an oscillating-blade tissue slicer. After 60 min incubation with normal or PANDAS sera (6.25 mg/dL) in standard ACSF containing (in mM): 128 NaCl, 3 KCl, 2 $CaCl_2$, 2 MgSO4, 24 NaHCO3, 1.25 NaH_2PO4, and 10 d-glucose (pH 7.35–7.38) was equilibrated with 95% O_2/5% CO_2 at RT, slices were transferred into a submerged recording chamber; bath temperature was then raised to 32 °C. Patch pipettes (3–5 MΩ) were pulled from glass tubing with a Flaming-Brown Horizontal Puller. The pipette solution contained the following (in mM): 115 K-gluconate, 5 KCl, 2 $MgCl_2$, 2 Mg-ATP, 2 Na_2-ATP, 10 Na_2-phosphocreatine, 0.4 Na_2-GTP, and 10 HEPES, pH 7.33. Neurobiotin (0.3%) was added to the pipette solution to mark cells for later imaging. All drugs, in ACSF, was applied for 1.5 min at a time in the fast-flowing bath, followed by a washout period of 8–10 min.

Cholinergic interneurons in striatum were visualized by videomicroscopy (40x IR lens) with infrared differential interference contrast (IR/DIC) and selected based on their size and characteristic morphology. Whole-cell recordings were performed with an Axoclamp-2B amplifier. Postsynaptic currents were studied in the continuous single-electrode voltage-clamp mode (3000 Hz low-pass filter) clamped at −70 mV. Spontaneous or neurotransmitter (5-HT, AMPA and dopamine)-evoked spike and intrinsic membrane properties were determine using current clamp. Analysis of spike frequency and inward current was conducted with Clampfit 10 software (Molecular Devices, Sunnyvale, CA).

Data analysis

All data are expressed as means ± SD. Statistical analyses were performed using SPSS Statistics 24 (IBM, New York, NY) or Prism 7.0 (GraphPad Software, La Jolla, California). Significance ($p<0.05$) was determined by two-tailed t-test (unpaired or paired), one-sample t-test, or one-way or two-way analysis of variance (ANOVA) with post-hoc Tukey's test. The specific test used in each analysis is listed in the figure legends. The unit of analysis (patient/serum, mouse, slice, or cell) is indicated for individual analyses. Pearson correlation was used to examine linear relationships between measures. For electrophysiology, the mean discharge frequency at 30 s before administration and 30 s after administration was compared and statistically analyzed.

RESULTS

PANDAS IgG shows specifically elevated binding to mouse striatal CINs

In a recent pilot study, we examined the binding of IgG from 5 children with PANDAS to striatal interneurons after infusion of human sera into the brains of mice *in vivo*, and found elevated binding specifically to CINs (21, 47). Here, we developed an *ex vivo* approach to replicate and extend this pilot work, equalizing IgG titers across samples and using blinded, unbiased imaging with automated scoring (see Methods).

We first tested the 5 PANDAS and 5 control samples characterized in our pilot study using this *ex vivo* assay; this constitutes a technical replication of our previous work (47). Mouse CINs were identified using an anti-choline acetyltransferase (ChAT) antibody; deposition of serum IgG onto these cells was visualized using a specific anti-human IgG antibody. IgG from both PANDAS and control sera binds to striatal mouse CINs (see Figures S4A and S16A). We quantified IgG immunofluorescence within all visualized ChAT-positive cells for each serum (400–800 cells/serum across multiple microscope fields). IgG immunofluorescence followed a normal distribution for each serum, but the distribution of binding by PANDAS antibodies was shifted to the right, indicating more deposition of PANDAS antibodies onto CINs (see Figure S4B). Comparison of mean CIN IgG immunofluorescence for each serum confirmed significantly higher antibody binding in the PANDAS group (see Figure S4C). *Ex vivo* binding scored in this way correlated positively though imperfectly with binding scored manually after *in vivo* infusion of the same sera in our previous work (r^2=0.373, p=0.061; not shown) (47). There was no between-group difference in ChAT immunofluorescence (data not shown), indicating that PANDAS and control sera did not differentially affect ChAT antibody binding.

Next, we investigated binding of serum IgG to other types of mouse interneuron. In PV-positive interneurons, PANDAS and control serum displayed similar IgG deposition (see Figures S4D, and S16B), with no between-group difference (see Figure S4E,F). Similarly, in nNOS-positive interneurons, PANDAS and control sera bound similarly (see Figures S4G–S4I and S16C). Together these results replicate our previous report that PANDAS serum IgG show selectively elevated binding to CINs in this small number of rigorously characterized patient samples (47).

Independent replication of binding of PANDAS IgG to CINs in two additional cohorts of patients.

To test the generality of this finding, we performed the same analyses in two independent groups of patients. The second cohort consisted of 6 children with PANDAS and 6 age- and sex-matched controls (Table S1, subjects 6–11). PANDAS cases were again drawn from a recent trial of IVIG treatment (21) and were selected to be clinical responders after either blinded or open-label IVIG. The third cohort consisted of 16 children with PANDAS and 12 age- and sex-matched controls collected by the same group (S.S. and the NIMH PANDAS clinic; see Table S2). Subjects in the third cohort were not selected to be treatment responders; indeed, many of them were not treated with IVIG. Consistent with the findings in the first 5 cases, IgG from both PANDAS and control sera binds to mouse striatal

CINs (Figure 1A). Combined data from all three cohorts (27 PANDAS and 23 control cases) showed a robust and significant group difference, with elevated binding of IgG from PANDAS samples relative to controls (Figure 1B). The level of ChAT immunofluorescence was unchanged between groups (Figure 1C), indicating no differential effect on anti-ChAT antibody binding. The number of ChAT-positive cells scored in the mouse striatum did not differ between PANDAS IgG and control IgG treated groups (see Figure S5A).

Binding of serum IgG to PV-positive interneurons did not differ between PANDAS patients and controls in pooled data from all three cohorts (Figure 1D). There was no difference between groups in the number of PV-positive cells or PV staining per cell (see Figures S5B and S5C in the data supplement).

To determine whether this elevated binding is seen in all cholinergic neurons, we next examined serum IgG binding to cholinergic neurons in the mouse medial septum. IgG immunofluorescence was seen in these cholinergic neurons (see Figure S16D), but there was no difference between groups (Figure 1F). There was no difference between groups in the number of ChAT-positive cells or the intensity of ChAT immunofluorescence per cell (see Figures S5D,E).

We also examined antibody binding of sera from the first and second cohorts (11 PANDAS and 11 control cases) to other cells in the striatum. IgG from PANDAS and control sera bound similarly to nNOS-expressing interneurons (FigureS6A). There was no difference between groups in the number of nNOS-positive cells or nNOS staining per cell (see Figures S6B,C). A few previous studies have suggested that PANDAS serum antibodies may bind to dopamine D1R and D2R receptors (8, 18). We tested whether IgG in PANDAS serum would show altered binding to striatal medium spiny neurons (MSNs) expressing D1R or D2R. To distinguish D1R- and D2R-expressing MSNs, we used double-transgenic mice expressing transgenic DARPP-32 with a FLAG epitope tag in $D1R^+$ MSNs and with a Myc epitope tag in $D2R^+$ MSNs (49), as in our recent work (50, 53). Double-labeling for epitope tags (FLAG or Myc) and human IgG (see Figures S17A,B) allows cell type-specific quantification of IgG binding, using the *ex vivo* approach described above for interneurons. Binding of IgG from PANDAS and control sera to $D1R^+$ MSNs (Figure S6D) and $D2R^+$ MSNs (Figure S6G) was equivalent. There was no difference between groups in FLAG or Myc staining per cell (Figure S6E,H) or the number of FLAG-positive or Myc-positive cells (Figures S6F,I). These controls, including three cell types not examined in our previous work (47) (septal cholinergic neurons, $D1R^+$ and $D2R^+$ MSNs), further confirm the specificity of elevated PANDAS antibody binding to CINs.

PANDAS IgG shows elevated binding to CINs, but not to PV-expressing interneurons in normal human brains

To confirm these findings in human brain, we examined the binding of IgG from PANDAS and control sera to slices of human basal ganglia of normal subjects. Pilot studies were carried out to optimize staining conditions (Figure S7). Sera from the first two cohorts (11 PANDAS and 11 control) were incubated with slices of human caudate and putamen and then co-immunostained for human IgG, ChAT, and PV. IgG binding to the CIN was elevated after incubation with PANDAS serum compared to the control serum in the caudate (Figures

2A,B) and putamen (Figures 2C,D). There was no between-group difference in IgG binding to PV-positive interneurons in the caudate (Figures 2E,F) or putamen (Figures 2G,H). Serum incubation did not alter ChAT or PV immunofluorescence (not shown).

PANDAS serum reduces CIN activity

CINs regulate motor function (54, 55) and are reduced in number *post mortem* in adults with Tourette syndrome (42, 43). Selective depletion of CINs in mice produces repetitive behavioral pathology (45, 56). We used phosphorylation levels of ribosomal protein S6 (rpS6) as a readout for CIN activity in mouse striatal slices acutely treated with control or PANDAS sera (see Figures S8, S9, and S18A) to test whether binding by PANDAS antibodies affects CIN function (as previously described (57). All values were normalized to P-rpS6 in CINs treated in parallel with saline.

We tested the 11 PANDAS sera and 11 matched control sera for modulation of CIN activity in this assay. Control serum did not significantly alter P-rpS6, relative to vehicle. PANDAS serum treatment significantly lowered P-rpS6 levels, relative to control serum (Figures 3A,B; see also Figure S18B). ChAT immunostaining was not significantly changed by serum treatment (Figure 3C), nor was the number of ChAT-positive cells (data not shown).

Across all 22 samples, serum IgG binding to CINs correlated negatively with CIN P-rpS6 activity after serum treatment (Figure 3D). The difference between PANDAS and control IgG binding to CINs in each age- and gender-matched serum pair correlated with the PANDAS-control difference in P-rpS6 after serum incubation (Figure 3E). These associations suggest that binding PANDAS IgG binding negatively regulates the activity of striatal CINs.

To test the specificity of this change, we investigated whether PANDAS serum affected the activity of PV-positive interneurons, again measured by immunostaining for P-rpS6 (58, 59), in striatal slices (see Figures S10 and S18C). PANDAS and control serum-treated striatal slices showed similar levels of P-rpS6 in PV-interneurons (Figures 3F and 3G; see also Figure S18D). Serum treatment did not alter PV immunostaining, relative to saline (Figure 3H). No correlation was found between serum IgG binding to PV-interneurons and P-rpS6 levels (Figure 3I), or between the difference between PANDAS and matched control IgG binding to PV-interneurons and the difference in PV P-rpS6 levels (Figure 3J).

PANDAS serum alters CIN electrophysiological responses

We used whole-cell patch recording to further examine the effect of PANDAS serum on CIN activity in acute slice. These experiments require much larger serum volumes than the immunostaining described above (Figure 3), and we were thus only able to conduct them with a single PANDAS-control serum pair for which we had adequate volume of serum. CINs were identified on the basis of their electrophysiological and morphological characteristics, including large somata and hyperpolarizing current pulses evoked a prominent voltage sag, characteristic of an I_h current (Figure S11A,B). Most recorded neurons displayed spontaneous spiking, with relatively broad action potentials (Figure S11C,D). PANDAS and control sera did not differentially affect intrinsic membrane properties of cholinergic interneurons (Table S4).

CINs receive various synaptic inputs, including glutamate, dopamine (DA), and serotonin (5-HT) (54). We therefore examined their response to bath application of agonists for these receptors. In slices pretreated with control serum, application of the ionotropic glutamate agonist AMPA produced a robust increase in action potential frequency in CINs, measured under current clamp. This increase did not occur in slices pretreated with PANDAS serum (Figure S12A,B). Alterations were also seen in the response of CINs to dopamine (DA) and serotonin (5-HT) after pretreatment with PANDAS serum (Figure S12C–F). Under voltage clamp, inward current was seen after application of all three agonists; the current induced by 5-HT was significantly reduced after pretreatment with PANDAS serum, while the response to AMPA and DA was not significantly altered (see Figure S13). These electrophysiological data must be interpreted with caution, as we were able to perform these assays with only a single serum pair; with that caveat, they support the molecular data (Figures 3,5) indicating that pretreatment with PANDAS serum can reduce the firing and/or responsivity of CINs *ex vivo*.

IVIG treatment reduces binding of PANDAS IgG to CINs

IVIG treatment has been reported to ameliorate symptoms in PANDAS, in some studies (19, 21, 60); the first two patient cohorts in the current study were selected on the basis of their response 6–12 weeks after either blinded or open-label IVIG treatment (Figure S1). We examined the correlation of change in CIN binding with change in symptoms after IVIG. In the original cohort of 5 patients, post-treatment serum showed a small but consistent reduction in antibody binding to CINs (Figure 4,B; see also Figure S19A). The pre-post treatment change of antibody binding to CINs correlated positively with symptom improvement (ΔCY-BOCS), at trend level (Figure 4C). This constitutes a technical replication of our previous work on these sera using an *in vivo* antibody binding assay (47).

We repeated this analysis in the second cohort of 6 PANDAS subjects and found a similar reduction in IgG binding to CINs after IVIG treatment (Figure 4D). The change of antibody binding to CINs correlated significantly with the change of CY-BOCS score in this second cohort (Figure 4E). In pooled data, IVIG significantly decreased IgG deposition onto CINs (Figure 4F). The decline in antibody binding correlated robustly with symptom improvement (Figure 4G).

To test the specificity of this change, we examined whether PANDAS IgG binding to other neurons would be altered after IVIG. There was no pre-post treatment change in IgG binding to striatal PV-positive neurons in the original cohort, the replication cohort, or the pooled data (see Figures S14B,D,F and S19B). There was no correlation between pre-post treatment change in IgG binding and change in CY-BOCS (see Figures S14C,E,G). Similarly, there was no alteration in IgG binding to cholinergic neurons in the medial septum after IVIG treatment (see Figures S14I,K,M and S19C), and no correlation between change in septal cholinergic neuron binding and change in CY-BOCS (see Figures S14J, S14L and S14N).

IVIG treatment and IgG depletion prevent the effect of PANDAS serum pretreatment on CIN activity in acute striatal slices

PANDAS serum-induced change in CIN activity (Figure 3) may be due to antibody binding to CINs (Figure 1) or to the activity of other factors in the serum. To investigate whether IgG binding is necessary, we repeated the treatment of acute brain slices with control and PANDAS sera (pre-IVIG, S1) with two additional experimental groups: matched post-IVIG PANDAS sera (post-IVIG, S3) and IgG-depleted pre-IVIG PANDAS sera ("S1-depleted", see Figure S15). PANDAS serum (S1) reduced P-rpS6 levels in striatal CINs relative to control serum (Figures 5A,B, replicating Figure 3B). The difference between PANDAS and control IgG binding to CINs (Figure 1) again correlated with the PANDAS-control difference in P-rpS6 after serum incubation (Figure 5C, replicating Figure 3E). In contrast, neither post-IVIG sera nor IgG-depleted baseline PANDAS serum reduce CIN P-rpS6 (Figure 5A,B). IgG binding of pre- and post-IVIG PANDAS sera (S1 and S3) to CINs correlated negatively with P-rpS6 levels after serum incubation (Figures 5D). The difference between IgG binding of baseline and post-IVIG treatment PANDAS serum correlated with the pre-post difference in P-rpS6 levels after serum incubation (Figure 5E).

We also examined P-rpS6 levels in PV-expressing interneurons after serum treatment. Again, we found no difference between control and PANDAS groups (Figures 5F–5H; compare to Figures 3G,J). Moreover, IVIG-treatment and IgG-depletion did not alter P-rpS6 levels in PV-interneurons (Figures 5F,G). No correlation was found between S1 and S3 sera IgG binding to PV-interneurons and P-rpS6 levels (Figure 5I), or between the difference of S1 and S3 IgG binding to PV-interneurons and the difference in P-rpS6 levels (Figure 5J). Serum treatment did not have any effect on ChAT or PV staining (data not shown).

DISCUSSION

An autoimmune pathophysiology has been proposed for PANDAS but remains unproven (5–7). While a number of possible pathogenic antibody targets have been described, none have been consistently replicated, and how the binding of antibodies to brain targets leads to symptoms remains unclear (8, 9, 15–18, 61–63). Our findings, here and in our previously published pilot study (47), reveal a hitherto unrecognized target for antibodies in these patients: the cholinergic interneurons (CINs) of the striatum. Our functional data (Figures 3 and 5) suggest that these antibodies can bind to CINs and reduce their activity, thereby disrupting the normal function of the corticostriatal circuitry.

Disruption of CINs has previously been implicated in Tourette syndrome, and in repetitive behavioral pathology more generally. Specifically, CINs are reduced in number in the striatum of adults with refractory Tourette syndrome (42, 43). Experimental depletion of these neurons in developmentally normal mice produces elevated grooming and repetitive behaviors, suggesting a causal relationship between this deficit and the development of relevant symptomatology (45, 46). These previous, independent results make CIN dysregulation an inherently plausible locus of pathology in PANDAS.

The consistency and specificity of elevated antibody binding to CINs, but not other examined cells, is striking. We find elevated IgG binding to mouse striatal CINs in 27

children with PANDAS, across three independent cohorts of patients, compared to age- and sex-matched controls (Figures 1B). In conjunction with our previous results (47), the effect has now been seen using two different experimental approaches (*in vivo* and *ex vivo* antibody delivery), with both confocal and standard fluorescent imaging, with two different quantification strategies, in three different primary experimenters' hands, with blinding to experimental condition. There is, with equal consistency, no elevated binding to two classes of GABAergic interneuron in the striatum (Figure 1D and S6A) (47). Moreover, we confirmed these findings in human brains: 11 PANDAS sera showed elevated IgG binding to CINs in both caudate and putamen, compared to matched controls (Figures 2B,D), with no difference between groups in IgG binding to PV-interneurons (Figures 2F,H). It is of course possible that differential binding to other cell types would be seen in a more exhaustive examination of different cell types throughout the brain; this is an important direction for future research.

We find no altered binding to D1- or D2-expressing medium spiny neurons (MSNs) of the striatum (see Figures S6D and S6G in the data supplement). Binding by PANDAS antibodies to both D1R and D2R dopamine receptors has been investigated previously, using *in vitro* binding to denatured protein (17, 18) or to heterologous cells overexpressing dopamine receptors (64). D2R dopamine receptors are present on CINs and thus could explain the elevated CIN binding that we see. The lack of any change in binding to D2R-expressing MSNs, however, argues against this possibility. We also see no elevated binding to cholinergic cells in the medial septum (Figure 1E), indicating that the abnormality does not generalize to cholinergic cells throughout the nervous system, or even the forebrain.

The specific molecular targets on striatal CINs that explain elevated binding by PANDAS IgG remain unclear. There may be a single molecular target on these cells that has eluded identification in previous studies, perhaps because it is present at low concentration in total striatal lysate (as CINs represent a small minority of the cells in the striatum). However, our experimental approach does not require that a single molecular target explain the observed binding in all patients; it is possible that there are multiple targets that can lead to similar binding patterns and similar pathophysiological effects in different patients. Such heterogeneity could further explain the lack of replication that has characterized efforts to identify specific antibodies on the basis of binding to specific molecules, rather than to cell types. We note that in these experiments (though not in our previous work, 47) tissue was permeabilized before application of serum and thus both cell surface and intracellular antigens are accessible; surface antigens may be more relevant pathophysiological targets *in vivo*. Identification of the molecular targets of antibody binding in individual sera is an important future direction for this work.

In the third cohort of PANDAS patients, who were not selected for IVIG response (and some of whom were not treated with IVIG at all), we find a similar but statistically weaker increase in IgG binding to CINs. The somewhat attenuated effect in this third cohort suggests that it may be more heterogeneous, containing some subjects with IgG-mediated pathology similar to that present in the first cohorts but others with a different pathophysiology. Identification of the clinical correlates of elevated IgG binding to CINs,

both in patients with PANDAS and in related diagnostic groups, is an important direction for future work.

We also show, for the first time, that PANDAS antibodies can affect CIN activity, providing critical support for the proposed pathophysiological mechanism. Specifically, we treated mouse striatal slices with PANDAS and control serum *ex vivo*, and we measured activity-dependent phosphorylation of ribosomal protein S6 (P-rpS6), a validated marker of neuronal activity in both CINs (57) and PV-expressing interneurons (58, 59). We find reduced P-rpS6 after treatment with 11 PANDAS sera, but not with matched control sera (Figure 3B). This effect is lost when IgG is depleted from PANDAS serum (Figure 5B), indicating that IgG binding is necessary for CIN inhibition. Importantly, there is no similar effect on PV-expressing interneurons (Figures 3G–3J), further emphasizing the specificity of the effects on CINs seen throughout our study. Of course, we cannot exclude the possibility that antibodies in PANDAS sera can have other effects on PV-expressing interneurons not captured by this assay, or on other cells elsewhere in the brain.

Antibody-modulating therapies such as IVIG and plasmapheresis have shown promise in the treatment of PANDAS in some studies, though not in all (19–22). Our first 2 patient cohorts were drawn from a recent controlled study of IVIG treatment (21) (Figure S1). This allowed testing of serum collected before and after treatment (47). We find that IgG binding to CINs is reduced after IVIG treatment, and that this change correlates robustly with symptom improvement (Figure 4). Similarly, post-IVIG serum does not reduce CIN activity (Figure 5B); the change in antibody binding correlates with the change in ability to reduce CIN activity. Critically, there is no change in binding to PV-expressing interneurons in the striatum or in cholinergic cells of the medial septum after IVIG treatment (Figure S14).

As an additional measure of neuronal activity, we examined CIN response to bath neurotransmitter treatment *ex vivo* after incubation with PANDAS or control serum. PANDAS serum significant attenuated AMPA-induced spike frequency (Figure S12A,B). This may explain reduced P-rpS6 after PANDAS treatment (Figures 3 and 5), to the extent that glutamate tone contributes to basal CIN firing in our *ex vivo* preparation. PANDAS serum also modulated cellular responses to both DA and 5-HT. We were only able to perform these electrophysiological experiments with a single serum pair, due to limited supplies of clinical serum and the relatively large amounts needed for these studies. Nevertheless, in conjunction with the P-rpS6 staining data across all 11 PANDAS samples and matched controls (Figure 3), these data indicate that PANDAS serum can reduce activity of CINs.

The downstream consequences of PANDAS IgG binding to CINs *in vivo* remain to be elucidated. We hypothesize that pathogenic PANDAS antibodies reduce CIN activity *in vivo*, as we have shown *ex vivo* (Figures 3 and 5; also see Figures S12 and S13). This may functionally parallel the effect of reduced CIN number in adults with severe TS (42, 43) and of experimental CIN disruption can produce repetitive behavioral pathology in mice (45). CINs have been shown to differentially regulate D1R-expressing MSNs of the striatonigral (direct) pathway and D2R-expressing MSNs of the striatopallidal (indirect)

pathway (65, 66) via muscarinic acetylcholine receptors (54, 67). The CINs interact with other neurotransmitter systems; they co-release glutamate (68) and drive dopamine and GABA release from dopamine terminals (69–71). CINs can also indirectly inhibit MSNs via their up regulation of GABAergic interneuron activity (72–75). Thus, inhibition of CINs may lead to dysregulated striatal output through several mechanisms.

Dysfunction of basal ganglia occurs commonly in other autoimmune encephalitides. Functional brain imaging studies show basal ganglia hypermetabolism in patients with autoimmune encephalitis (76, 77). In anti-N-methyl-D-aspartate (NMDA) receptor encephalitis, loss of cortico-striatal inhibition due to antibody-mediated inhibition of GABAergic interneurons has been postulated (78–80). In another rare autoimmune disorder, stiff-person syndrome, anti-GAD65 (81) and anti-amphiphysin (82) autoantibodies disrupt GABAergic inhibitory synaptic activity, which may underlie the pathophysiological mechanisms of this disorder. Our findings suggest that a similar mechanism may be at play in PANDAS, with antibody binding to interneurons leading to an imbalance between excitatory and inhibitory synaptic transmission in the basal ganglia and thus to clinical symptoms. Importantly, we have not shown antibody binding to CINs to be specific to PANDAS; indeed, since PANDAS is a clinical entity and diagnosis is not based on a clearly defined underlying pathophysiology, we think it unlikely that elevated CIN binding will correspond precisely with clinical diagnosis. This binding pattern may not be seen in all patients with a PANDAS diagnosis (as suggested by the overlap of PANDAS and control values in Figure 1), and a similar pathophysiology may contribute to other neuroinflammatory conditions. Systematic examination of interneuron binding across psychiatric and neurological diagnoses is an important future direction; such an examination will be facilitated by the identification of the associated molecular targets.

The current work tests PANDAS IgG binding to fixed mouse striatal slices, and human brain tissue, *ex vivo*. This differs from the *in vivo* infusion used in our pilot work (47). These two strategies ask subtly different questions. *In vivo* antibody infusion demonstrates that antibodies in PANDAS sera can bind to CINs in intact brain, under physiological conditions, over days. The current *ex vivo* approach is less chronic, examining binding after an overnight incubation (Figures 1, 2, 4), and functional effects after only 1 hour (Figures 3, 5; see also Figures S12, S13). It allows better control of IgG concentration, which may vary between animals *in vivo*. It is less laborious, which allows for analysis of larger numbers of samples and the inclusion of additional controls. Importantly, the *ex vivo* approach permits, for the first time, examination of the functional effects of PANDAS serum on CIN activity (Figures 3, 5; see also Figures S12, S13).

We have also used an automated method to quantify IgG binding to CINs, and other neuronal types (see Figure S2 in the data supplement), which contrasts to the blinded manual counting used in our pilot work (47). This allows us to count an order of magnitude more cells than previously. On the other hand, the effect size of the elevated binding of IgG to CINs in our pilot work (d=8.1) was much higher than what we see here (d=1.8 in the first cohort and somewhat less in the others). The use of standard fluorescent imaging rather than confocal imaging, which allows us to count more cells at lower magnification, leads to higher background, which doubtless contributes to this smaller (though still large)

effect size. Lower background in the *in vivo* work may also derive from the more chronic serum administration and the 5-day clearance period after antibody infusion (47), which may produce better signal-to-noise. Additionally, in our previous work we categorized individual cells as either positive or negative for IgG, which is an inherently nonlinear approach and may amplify between-group effects. The finding of qualitatively identical results using these two experimental approaches, despite these differences, increases confidence in the finding.

There are, of course, several limitations to this study. The sera are as clinically homogeneous as we could achieve, especially in the first two patient cohorts, with rigorous PANDAS diagnosis and a narrow age range. These design choices were made to maximize our ability to find a pathophysiological signal in a small, homogeneous sample, which can subsequently be investigated in more heterogeneous populations. This approach has been fruitful in investigations of other autoimmune neural pathologies (83). We have examined binding to both mouse and human striatal tissue, but in both cases this tissue was from adults; it is possible that more or different binding would be seen on pediatric tissue. We have focused on a specific brain region (the striatum) and on specific cell types, based on *a priori* considerations; it is possible that a more comprehensive survey would additionally reveal elevated binding by PANDAS IgG to other cells in other brain regions. And we have focused on the ability of IgG to bind to interneurons but have not addressed the question of how these antibodies could access the brain in patients; this is an important, though distinct, topic for future research.

While the finding of elevated IgG binding to CINs documented here represents an exciting new insight into possible pathophysiological mechanisms in PANDAS, it would be premature to consider this a clinical assay. Overlap between PANDAS and control groups is substantial (Figure 1B), and the specificity and prognostic utility of elevated CIN binding remain to be established. Development of a diagnostic assay based on these results may require the identification of the molecular target(s) of antibody binding to CINs. This is an important future direction. Ultimately, the identification and replication of specific binding targets, and clarification of their relationship to particular patterns of symptomatology or of treatment response, may help to clarify the diagnostic landscape in PANDAS and PANS, in addition to providing clinically useful laboratory tests.

In conclusion, we find PANDAS antibodies to show elevated binding to striatal CINs but not several other neuronal types (47), to decline in parallel with symptom improvement after IVIG treatment, and to reduce the activity of CINs, and perhaps to alter their response to several neurotransmitters, *ex vivo*. This supports a novel hypothesis for the pathophysiology of PANDAS that suggests important directions for future research. Identifying cellular targets of pathogenic antibodies in PANDAS holds promise for validation of the diagnosis and for identification of targets for future treatment development.

Supplementary Material

Refer to Web version on PubMed Central for supplementary material.

Acknowledgements

This work was funded by NIH grants R01NS101104 and R21MH109700 and NIH contract HHSN271201800709P (CP), by the NIMH intramural research program through its support of SS, and by The Avielle Foundation through its support of SF. The State of Connecticut also supported this study via its support of the Ribicoff Research Facilities at the Connecticut Mental Health Center. We thank Jessica Lennington for assistance with human tissue processing, Margaret Pekar and Betsy D'Amico for assistance with serum handling and organization, Betsy D'Amico for mouse genotyping and management, and other laboratory members for helpful discussions and critical reading of the manuscript.

REFERENCES

1. Weissman MM, Bland RC, Canino GJ, Greenwald S, Hwu HG, Lee CK, Newman SC, Oakley-Browne MA, Rubio-Stipec M, Wickramaratne PJ, et al. The cross national epidemiology of obsessive compulsive disorder. The Cross National Collaborative Group. J Clin Psychiatry. 1994;55 Suppl:5–10.
2. Ruscio AM, Stein DJ, Chiu WT, Kessler RC. The epidemiology of obsessive-compulsive disorder in the National Comorbidity Survey Replication. Mol Psychiatry. 2010;15:53–63. [PubMed: 18725912]
3. SE S, JF L, NR R. From Research Subgroup to Clinical Syndrome: Modifying the PANDAS Criteria to Describe PANS (Pediatric Acute-onset Neuropsychiatric Syndrome). 2012;2:113.
4. Singer HS, Gilbert DL, Wolf DS, Mink JW, Kurlan R. Moving from PANDAS to CANS. J Pediatr. 2012;160:725–731. [PubMed: 22197466]
5. Swedo SE, Leonard HL, Garvey M, Mittleman B, Allen AJ, Perlmutter S, Lougee L, Dow S, Zamkoff J, Dubbert BK. Pediatric autoimmune neuropsychiatric disorders associated with streptococcal infections: clinical description of the first 50 cases. Am J Psychiatry. 1998;155:264–271. [PubMed: 9464208]
6. Murphy TK, Patel PD, McGuire JF, Kennel A, Mutch PJ, Parker-Athill EC, Hanks CE, Lewin AB, Storch EA, Toufexis MD, Dadlani GH, Rodriguez CA. Characterization of the pediatric acute-onset neuropsychiatric syndrome phenotype. J Child Adolesc Psychopharmacol. 2015;25:14–25. [PubMed: 25314221]
7. Chang K, Frankovich J, Cooperstock M, Cunningham MW, Latimer ME, Murphy TK, Pasternack M, Thienemann M, Williams K, Walter J, Swedo SE. Clinical evaluation of youth with pediatric acute-onset neuropsychiatric syndrome (PANS): recommendations from the 2013 PANS Consensus Conference. J Child Adolesc Psychopharmacol. 2015;25:3–13. [PubMed: 25325534]
8. Kirvan CA, Swedo SE, Heuser JS, Cunningham MW. Mimicry and autoantibody-mediated neuronal cell signaling in Sydenham chorea. Nat Med. 2003;9:914–920. [PubMed: 12819778]
9. Kirvan CA, Swedo SE, Kurahara D, Cunningham MW. Streptococcal mimicry and antibody-mediated cell signaling in the pathogenesis of Sydenham's chorea. Autoimmunity. 2006;39:21–29. [PubMed: 16455579]
10. Swedo SE. Sydenham's chorea. A model for childhood autoimmune neuropsychiatric disorders. JAMA. 1994;272:1788–1791. [PubMed: 7661914]
11. Swedo SE, Rapoport JL, Cheslow DL, Leonard HL, Ayoub EM, Hosier DM, Wald ER. High prevalence of obsessive-compulsive symptoms in patients with Sydenham's chorea. Am J Psychiatry. 1989;146:246–249. [PubMed: 2912267]
12. Asbahr FR, Garvey MA, Snider LA, Zanetta DM, Elkis H, Swedo SE. Obsessive-compulsive symptoms among patients with Sydenham chorea. Biol Psychiatry. 2005;57:1073–1076. [PubMed: 15860349]
13. Witebsky E, Rose NR, Terplan K, Paine JR, Egan RW. Chronic thyroiditis and autoimmunization. J Am Med Assoc. 1957;164:1439–1447. [PubMed: 13448890]
14. Rose NR, Bona C. Defining criteria for autoimmune diseases (Witebsky's postulates revisited). Immunol Today. 1993;14:426–430. [PubMed: 8216719]
15. Kirvan CA, Swedo SE, Snider LA, Cunningham MW. Antibody-mediated neuronal cell signaling in behavior and movement disorders. J Neuroimmunol. 2006;179:173–179. [PubMed: 16875742]

16. Kirvan CA, Cox CJ, Swedo SE, Cunningham MW. Tubulin is a neuronal target of autoantibodies in Sydenham's chorea. J Immunol. 2007;178:7412–7421. [PubMed: 17513792]
17. Ben-Pazi H, Stoner JA, Cunningham MW. Dopamine receptor autoantibodies correlate with symptoms in Sydenham's chorea. PLoS One. 2013;8:e73516. [PubMed: 24073196]
18. Cox CJ, Sharma M, Leckman JF, Zuccolo J, Zuccolo A, Kovoor A, Swedo SE, Cunningham MW. Brain human monoclonal autoantibody from sydenham chorea targets dopaminergic neurons in transgenic mice and signals dopamine D2 receptor: implications in human disease. J Immunol. 2013;191:5524–5541. [PubMed: 24184556]
19. Perlmutter SJ, Leitman SF, Garvey MA, Hamburger S, Feldman E, Leonard HL, Swedo SE. Therapeutic plasma exchange and intravenous immunoglobulin for obsessive-compulsive disorder and tic disorders in childhood. Lancet. 1999;354:1153–1158. [PubMed: 10513708]
20. Garvey MA, Snider LA, Leitman SF, Werden R, Swedo SE. Treatment of Sydenham's chorea with intravenous immunoglobulin, plasma exchange, or prednisone. J Child Neurol. 2005;20:424–429. [PubMed: 15968928]
21. Williams KA, Swedo SE, Farmer CA, Grantz H, Grant PJ, D'Souza P, Hommer R, Katsovich L, King RA, Leckman JF. Randomized, Controlled Trial of Intravenous Immunoglobulin for Pediatric Autoimmune Neuropsychiatric Disorders Associated With Streptococcal Infections. J Am Acad Child Adolesc Psychiatry. 2016;55:860–867. [PubMed: 27663941]
22. Sigra S, Hesselmark E, Bejerot S. Treatment of PANDAS and PANS: a systematic review. Neurosci Biobehav Rev. 2018;86:51–65. [PubMed: 29309797]
23. Snider LA, Lougee L, Slattery M, Grant P, Swedo SE. Antibiotic prophylaxis with azithromycin or penicillin for childhood-onset neuropsychiatric disorders. Biol Psychiatry. 2005;57:788–792. [PubMed: 15820236]
24. Garvey MA, Perlmutter SJ, Allen AJ, Hamburger S, Lougee L, Leonard HL, Witowski ME, Dubbert B, Swedo SE. A pilot study of penicillin prophylaxis for neuropsychiatric exacerbations triggered by streptococcal infections. Biol Psychiatry. 1999;45:1564–1571. [PubMed: 10376116]
25. Kurlan R, Kaplan EL. The pediatric autoimmune neuropsychiatric disorders associated with streptococcal infection (PANDAS) etiology for tics and obsessive-compulsive symptoms: hypothesis or entity? Practical considerations for the clinician. Pediatrics. 2004;113:883–886. [PubMed: 15060240]
26. Yaddanapudi K, Hornig M, Serge R, De Miranda J, Baghban A, Villar G, Lipkin WI. Passive transfer of streptococcus-induced antibodies reproduces behavioral disturbances in a mouse model of pediatric autoimmune neuropsychiatric disorders associated with streptococcal infection. Mol Psychiatry. 2010;15:712–726. [PubMed: 19668249]
27. Lotan D, Benhar I, Alvarez K, Mascaro-Blanco A, Brimberg L, Frenkel D, Cunningham MW, Joel D. Behavioral and neural effects of intra-striatal infusion of anti-streptococcal antibodies in rats. Brain Behav Immun. 2014;38:249–262. [PubMed: 24561489]
28. Pauls DL, Abramovitch A, Rauch SL, Geller DA. Obsessive-compulsive disorder: an integrative genetic and neurobiological perspective. Nat Rev Neurosci. 2014;15:410–424. [PubMed: 24840803]
29. Fernandez TV, Leckman JF, Pittenger C. Genetic susceptibility in obsessive-compulsive disorder. Handb Clin Neurol. 2018;148:767–781. [PubMed: 29478613]
30. Menzies L, Chamberlain SR, Laird AR, Thelen SM, Sahakian BJ, Bullmore ET. Integrating evidence from neuroimaging and neuropsychological studies of obsessive-compulsive disorder: the orbitofronto-striatal model revisited. Neurosci Biobehav Rev. 2008;32:525–549. [PubMed: 18061263]
31. Bostan AC, Strick PL. The basal ganglia and the cerebellum: nodes in an integrated network. Nat Rev Neurosci. 2018;19:338–350. [PubMed: 29643480]
32. Harrison BJ, Soriano-Mas C, Pujol J, Ortiz H, Lopez-Sola M, Hernandez-Ribas R, Deus J, Alonso P, Yucel M, Pantelis C, Menchon JM, Cardoner N. Altered corticostriatal functional connectivity in obsessive-compulsive disorder. Arch Gen Psychiatry. 2009;66:1189–1200. [PubMed: 19884607]
33. Radua J, Mataix-Cols D. Voxel-wise meta-analysis of grey matter changes in obsessive-compulsive disorder. Br J Psychiatry. 2009;195:393–402. [PubMed: 19880927]

34. Pittenger C, Bloch MH, Williams K. Glutamate abnormalities in obsessive compulsive disorder: neurobiology, pathophysiology, and treatment. Pharmacol Ther. 2011;132:314–332. [PubMed: 21963369]
35. Anticevic A, Hu S, Zhang S, Savic A, Billingslea E, Wasylink S, Repovs G, Cole MW, Bednarski S, Krystal JH, Bloch MH, Li CS, Pittenger C. Global resting-state functional magnetic resonance imaging analysis identifies frontal cortex, striatal, and cerebellar dysconnectivity in obsessive-compulsive disorder. Biol Psychiatry. 2014;75:595–605. [PubMed: 24314349]
36. Gerfen CR, Bolam JP. The Neuroanatomical Organization of the Basal Ganglia. Hbk Behav Neurosci. 2010;20:3–28.
37. Kreitzer AC. Physiology and pharmacology of striatal neurons. Annu Rev Neurosci. 2009;32:127–147. [PubMed: 19400717]
38. Tepper JM, Bolam JP. Functional diversity and specificity of neostriatal interneurons. Curr Opin Neurobiol. 2004;14:685–692. [PubMed: 15582369]
39. Apicella P Leading tonically active neurons of the striatum from reward detection to context recognition. Trends Neurosci. 2007;30:299–306. [PubMed: 17420057]
40. Burguiere E, Monteiro P, Mallet L, Feng G, Graybiel AM. Striatal circuits, habits, and implications for obsessive-compulsive disorder. Curr Opin Neurobiol. 2015;30:59–65. [PubMed: 25241072]
41. Rapanelli M, Frick LR, Pittenger C. The Role of Interneurons in Autism and Tourette Syndrome. Trends Neurosci. 2017;40:397–407. [PubMed: 28578790]
42. Kataoka Y, Kalanithi PS, Grantz H, Schwartz ML, Saper C, Leckman JF, Vaccarino FM. Decreased number of parvalbumin and cholinergic interneurons in the striatum of individuals with Tourette syndrome. J Comp Neurol. 2010;518:277–291. [PubMed: 19941350]
43. Lennington JB, Coppola G, Kataoka-Sasaki Y, Fernandez TV, Palejev D, Li Y, Huttner A, Pletikos M, Sestan N, Leckman JF, Vaccarino FM. Transcriptome Analysis of the Human Striatum in Tourette Syndrome. Biol Psychiatry. 2016;79:372–382. [PubMed: 25199956]
44. Kalanithi PS, Zheng W, Kataoka Y, DiFiglia M, Grantz H, Saper CB, Schwartz ML, Leckman JF, Vaccarino FM. Altered parvalbumin-positive neuron distribution in basal ganglia of individuals with Tourette syndrome. Proc Natl Acad Sci U S A. 2005;102:13307–13312. [PubMed: 16131542]
45. Xu M, Kobets A, Du JC, Lennington J, Li L, Banasr M, Duman RS, Vaccarino FM, DiLeone RJ, Pittenger C. Targeted ablation of cholinergic interneurons in the dorsolateral striatum produces behavioral manifestations of Tourette syndrome. Proc Natl Acad Sci U S A. 2015;112:893–898. [PubMed: 25561540]
46. Rapanelli M, Frick LR, Xu M, Groman SM, Jindachomthong K, Tamamaki N, Tanahira C, Taylor JR, Pittenger C. Targeted Interneuron Depletion in the Dorsal Striatum Produces Autism-like Behavioral Abnormalities in Male but Not Female Mice. Biol Psychiatry. 2017;82:194–203. [PubMed: 28347488]
47. Frick LR, Rapanelli M, Jindachomthong K, Grant P, Leckman JF, Swedo S, Williams K, Pittenger C. Differential binding of antibodies in PANDAS patients to cholinergic interneurons in the striatum. Brain Behav Immun. 2018;69:304–311. [PubMed: 29233751]
48. Scahill L, Riddle MA, McSwiggin-Hardin M, Ort SI, King RA, Goodman WK, Cicchetti D, Leckman JF. Children's Yale-Brown Obsessive Compulsive Scale: reliability and validity. J Am Acad Child Adolesc Psychiatry. 1997;36:844–852. [PubMed: 9183141]
49. Bateup HS, Svenningsson P, Kuroiwa M, Gong S, Nishi A, Heintz N, Greengard P. Cell type-specific regulation of DARPP-32 phosphorylation by psychostimulant and antipsychotic drugs. Nat Neurosci. 2008;11:932–939. [PubMed: 18622401]
50. Rapanelli M, Frick L, Jindachomthong K, Xu J, Ohtsu H, Nairn AC, Pittenger C. Striatal Signaling Regulated by the H3R Histamine Receptor in a Mouse Model of tic Pathophysiology. Neuroscience. 2018;392:172–179. [PubMed: 30278251]
51. Ting JT, Daigle TL, Chen Q, Feng G. Acute brain slice methods for adult and aging animals: application of targeted patch clamp analysis and optogenetics. Methods Mol Biol. 2014;1183:221–242. [PubMed: 25023312]
52. Liu RJ, Aghajanian GK. Stress blunts serotonin- and hypocretin-evoked EPSCs in prefrontal cortex: role of corticosterone-mediated apical dendritic atrophy. Proc Natl Acad Sci U S A. 2008;105:359–364. [PubMed: 18172209]

53. Rapanelli M, Frick LR, Horn KD, Schwarcz RC, Pogorelov V, Nairn AC, Pittenger C. The Histamine H3 Receptor Differentially Modulates Mitogen-activated Protein Kinase (MAPK) and Akt Signaling in Striatonigral and Striatopallidal Neurons. J Biol Chem. 2016;291:21042–21052. [PubMed: 27510032]
54. Lim SA, Kang UJ, McGehee DS. Striatal cholinergic interneuron regulation and circuit effects. Front Synaptic Neurosci. 2014;6:22. [PubMed: 25374536]
55. Gonzales KK, Smith Y. Cholinergic interneurons in the dorsal and ventral striatum: anatomical and functional considerations in normal and diseased conditions. Ann N Y Acad Sci. 2015;1349:1–45. [PubMed: 25876458]
56. Martos YV, Braz BY, Beccaria JP, Murer MG, Belforte JE. Compulsive Social Behavior Emerges after Selective Ablation of Striatal Cholinergic Interneurons. J Neurosci. 2017;37:2849–2858. [PubMed: 28193688]
57. Bertran-Gonzalez J, Chieng BC, Laurent V, Valjent E, Balleine BW. Striatal cholinergic interneurons display activity-related phosphorylation of ribosomal protein S6. PLoS One. 2012;7:e53195. [PubMed: 23285266]
58. Knight ZA, Tan K, Birsoy K, Schmidt S, Garrison JL, Wysocki RW, Emiliano A, Ekstrand MI, Friedman JM. Molecular profiling of activated neurons by phosphorylated ribosome capture. Cell. 2012;151:1126–1137. [PubMed: 23178128]
59. Pirbhoy PS, Farris S, Steward O. Synaptic activation of ribosomal protein S6 phosphorylation occurs locally in activated dendritic domains. Learn Mem. 2016;23:255–269. [PubMed: 27194793]
60. Kovacevic M, Grant P, Swedo SE. Use of intravenous immunoglobulin in the treatment of twelve youths with pediatric autoimmune neuropsychiatric disorders associated with streptococcal infections. J Child Adolesc Psychopharmacol. 2015;25:65–69. [PubMed: 25658609]
61. Singer HS, Hong JJ, Yoon DY, Williams PN. Serum autoantibodies do not differentiate PANDAS and Tourette syndrome from controls. Neurology. 2005;65:1701–1707. [PubMed: 16207842]
62. Morris CM, Pardo-Villamizar C, Gause CD, Singer HS. Serum autoantibodies measured by immunofluorescence confirm a failure to differentiate PANDAS and Tourette syndrome from controls. J Neurol Sci. 2009;276:45–48. [PubMed: 18823914]
63. Brilot F, Merheb V, Ding A, Murphy T, Dale RC. Antibody binding to neuronal surface in Sydenham chorea, but not in PANDAS or Tourette syndrome. Neurology. 2011;76:1508–1513. [PubMed: 21411742]
64. Dale RC, Merheb V, Pillai S, Wang D, Cantrill L, Murphy TK, Ben-Pazi H, Varadkar S, Aumann TD, Horne MK, Church AJ, Fath T, Brilot F. Antibodies to surface dopamine-2 receptor in autoimmune movement and psychiatric disorders. Brain. 2012;135:3453–3468. [PubMed: 23065479]
65. Nelson AB, Kreitzer AC. Reassessing models of basal ganglia function and dysfunction. Annu Rev Neurosci. 2014;37:117–135. [PubMed: 25032493]
66. Lanciego JL, Luquin N, Obeso JA. Functional neuroanatomy of the basal ganglia. Cold Spring Harb Perspect Med. 2012;2:a009621. [PubMed: 23071379]
67. Ding JB, Guzman JN, Peterson JD, Goldberg JA, Surmeier DJ. Thalamic gating of corticostriatal signaling by cholinergic interneurons. Neuron. 2010;67:294–307. [PubMed: 20670836]
68. Higley MJ, Gittis AH, Oldenburg IA, Balthasar N, Seal RP, Edwards RH, Lowell BB, Kreitzer AC, Sabatini BL. Cholinergic interneurons mediate fast VGluT3-dependent glutamatergic transmission in the striatum. PLoS One. 2011;6:e19155. [PubMed: 21544206]
69. Nelson AB, Hammack N, Yang CF, Shah NM, Seal RP, Kreitzer AC. Striatal cholinergic interneurons Drive GABA release from dopamine terminals. Neuron. 2014;82:63–70. [PubMed: 24613418]
70. Zhou FM, Liang Y, Dani JA. Endogenous nicotinic cholinergic activity regulates dopamine release in the striatum. Nat Neurosci. 2001;4:1224–1229. [PubMed: 11713470]
71. Threlfell S, Lalic T, Platt NJ, Jennings KA, Deisseroth K, Cragg SJ. Striatal dopamine release is triggered by synchronized activity in cholinergic interneurons. Neuron. 2012;75:58–64. [PubMed: 22794260]

72. Koos T, Tepper JM. Dual cholinergic control of fast-spiking interneurons in the neostriatum. J Neurosci. 2002;22:529–535. [PubMed: 11784799]

73. English DF, Ibanez-Sandoval O, Stark E, Tecuapetla F, Buzsaki G, Deisseroth K, Tepper JM, Koos T. GABAergic circuits mediate the reinforcement-related signals of striatal cholinergic interneurons. Nat Neurosci. 2011;15:123–130. [PubMed: 22158514]

74. Faust TW, Assous M, Tepper JM, Koos T. Neostriatal GABAergic Interneurons Mediate Cholinergic Inhibition of Spiny Projection Neurons. J Neurosci. 2016;36:9505–9511. [PubMed: 27605623]

75. Faust TW, Assous M, Shah F, Tepper JM, Koos T. Novel fast adapting interneurons mediate cholinergic-induced fast GABAA inhibitory postsynaptic currents in striatal spiny neurons. Eur J Neurosci. 2015;42:1764–1774. [PubMed: 25865337]

76. Maeder-Ingvar M, Prior JO, Irani SR, Rey V, Vincent A, Rossetti AO. FDG-PET hyperactivity in basal ganglia correlating with clinical course in anti-NDMA-R antibodies encephalitis. J Neurol Neurosurg Psychiatry. 2011;82:235–236. [PubMed: 20667855]

77. Turpin S, Martineau P, Levasseur MA, Meijer I, Decarie JC, Barsalou J, Renaud C, Decaluwe H, Haddad E, Lambert R. 18F-Flurodeoxyglucose positron emission tomography with computed tomography (FDG PET/CT) findings in children with encephalitis and comparison to conventional imaging. Eur J Nucl Med Mol Imaging. 2019;46:1309–1324. [PubMed: 30863933]

78. Kleinig TJ, Thompson PD, Matar W, Duggins A, Kimber TE, Morris JG, Kneebone CS, Blumbergs PC. The distinctive movement disorder of ovarian teratoma-associated encephalitis. Mov Disord. 2008;23:1256–1261. [PubMed: 18442127]

79. Dalmau J, Gleichman AJ, Hughes EG, Rossi JE, Peng X, Lai M, Dessain SK, Rosenfeld MR, Balice-Gordon R, Lynch DR. Anti-NMDA-receptor encephalitis: case series and analysis of the effects of antibodies. Lancet Neurol. 2008;7:1091–1098. [PubMed: 18851928]

80. Mohammad SS, Fung VS, Grattan-Smith P, Gill D, Pillai S, Ramanathan S, Brilot F, Dale RC. Movement disorders in children with anti-NMDAR encephalitis and other autoimmune encephalopathies. Mov Disord. 2014;29:1539–1542. [PubMed: 25154478]

81. Blum P, Jankovic J. Stiff-person syndrome: an autoimmune disease. Mov Disord. 1991;6:12–20. [PubMed: 2005917]

82. Geis C, Weishaupt A, Hallermann S, Grunewald B, Wessig C, Wultsch T, Reif A, Byts N, Beck M, Jablonka S, Boettger MK, Uceyler N, Fouquet W, Gerlach M, Meinck HM, Siren AL, Sigrist SJ, Toyka KV, Heckmann M, Sommer C. Stiff person syndrome-associated autoantibodies to amphiphysin mediate reduced GABAergic inhibition. Brain. 2010;133:3166–3180. [PubMed: 20884644]

83. Fujihara K. Neuromyelitis optica spectrum disorders: still evolving and broadening. Curr Opin Neurol. 2019;32:385–394. [PubMed: 30893099]

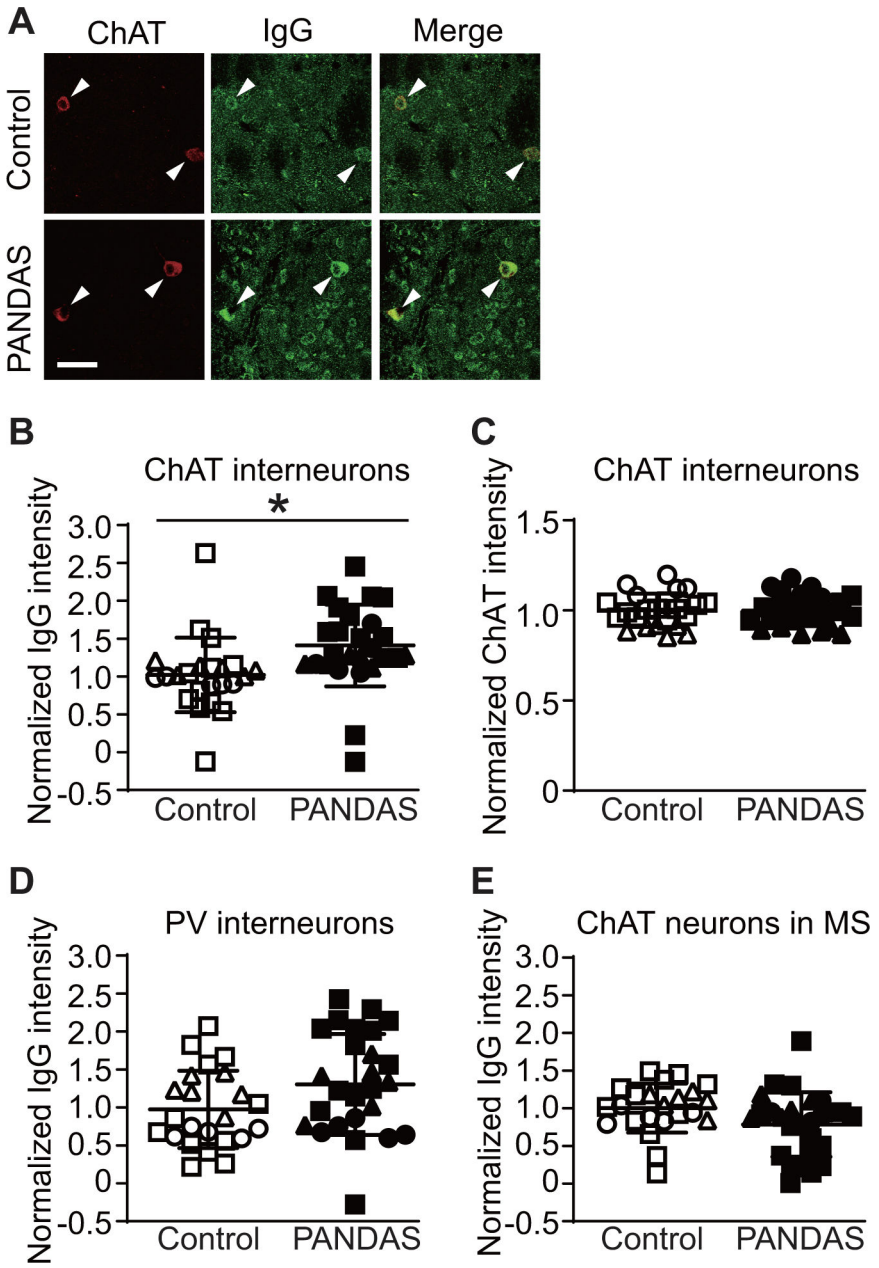

FIGURE 1. PANDAS IgG shows elevated binding to mouse striatal cholinergic interneurons.

(A) Illustrative confocal images of immunohistochemical staining of human IgG (green) and choline acetyltransferase (ChAT, red). Arrowheads indicate human IgG binding to ChAT-positive neurons (cholinergic interneurons, CINs). Scale bar: 40 μm. (B) Average intensity of IgG binding to CINs was higher after incubation with PANDAS sera than after incubation with control sera (2-tailed independent sample t-test: t[48]=2.654, p=0.011). This was true in separate analyses of each of the three cohorts of patients (cohort 1: t[8]=2.810, p=0.023; cohort 2: t[10]=2.785, p=0.019; cohort 3: t[26]=1.958, p=0.061). (C) Mean intensity of ChAT immunofluorescence did not differ between both groups (t[48]=0.067, p>0.9). (D and E) Serum IgG binding to several other neuron types did not significantly differ between PANDAS and control groups: (D) parvalbumin (PV)-expressing interneurons (t[48]=1.747,

p=0.087); (E) ChAT positive neurons in the medial septum (t[48]=1.717, p=0.093). *p<0.05; N=27 for PANDAS group and N=23 for control group. ●, ◯ – 10 serum from the first cohort (47); ▲, △ – 12 sera from the second cohort; ■, □ – 28 sera from the third cohort.

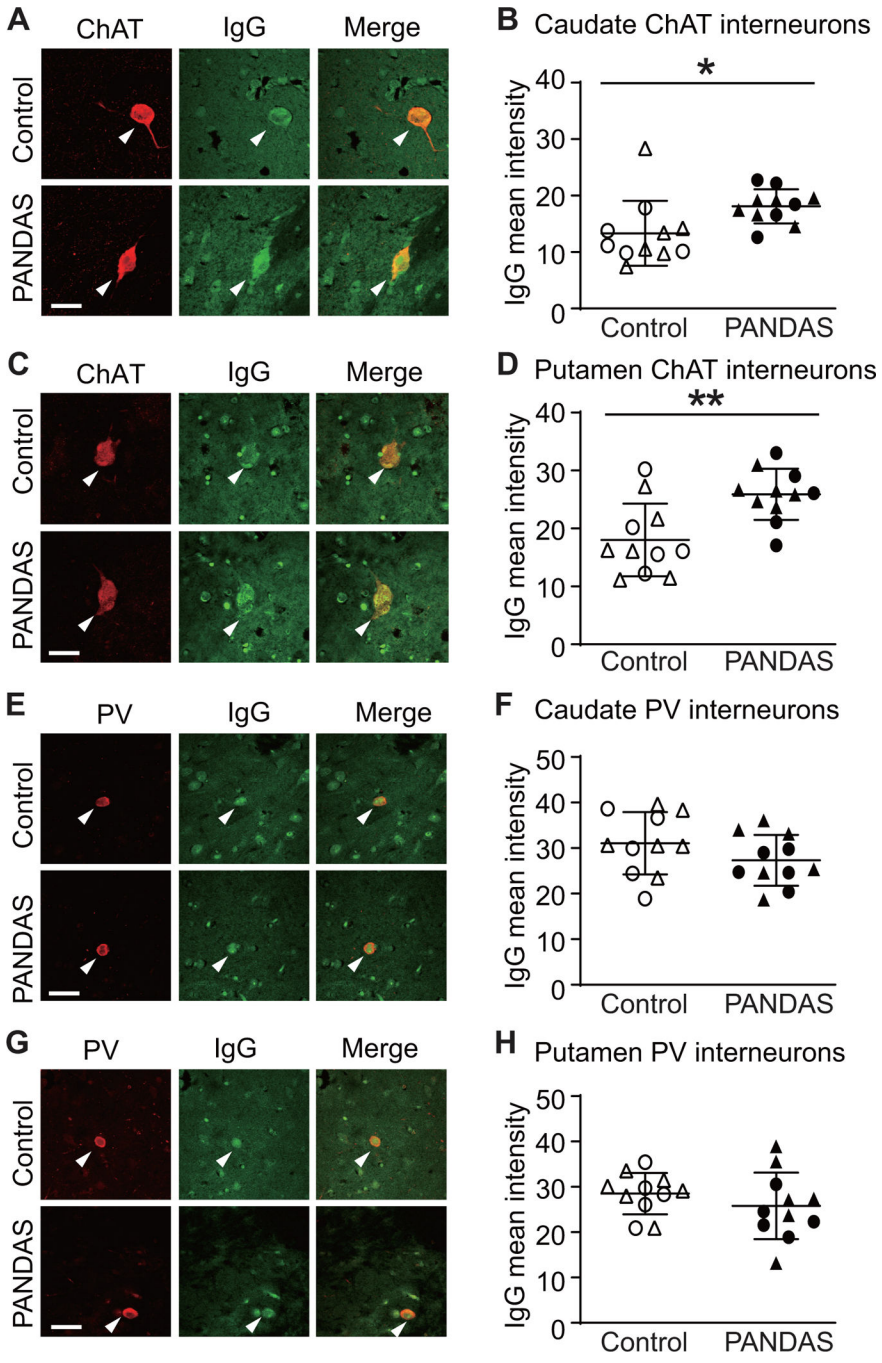

Figure 2. PANDAS IgG shows elevated binding to cholinergic interneurons in human brain slices.

(A and C) Representative confocal images of immunohistochemical staining of human IgG (green) and choline acetyltransferase (ChAT, red) in human caudate (A) and putamen (C). Arrowheads indicate human IgG binding to CINs. Scale bar: 40 μm. (B and D) PANDAS antibodies show more binding to CINs in human caudate (B) and putamen (D), relative to matched controls, as quantified by average fluorescence intensity: (B) in caudate ($t[20]=2.440$, $p=0.024$); (D) in putamen ($t[20]=3.401$, $p=0.003$). (E and G) Representative confocal images of immunohistochemical staining of human IgG (green) and parvalbumin

(PV, red) in human caudate (E) and putamen (G). Arrowheads indicate human IgG binding to PV-positive interneurons. Scale bar: 40 μm. (F and H) PANDAS antibodies do not show elevated binding to PV-positive interneurons: (F) in caudate ($t[20]=1.409$, $p=0.174$); (H) in putamen ($t[20]=1.042$, $p>0.3$). All comparisons are by independent samples t-test; *$p<0.05$, **$p<0.01$; N=11 each group. ●,◯ – 10 serum from the first cohort (47); ▲,△ – 12 sera from the second cohort.

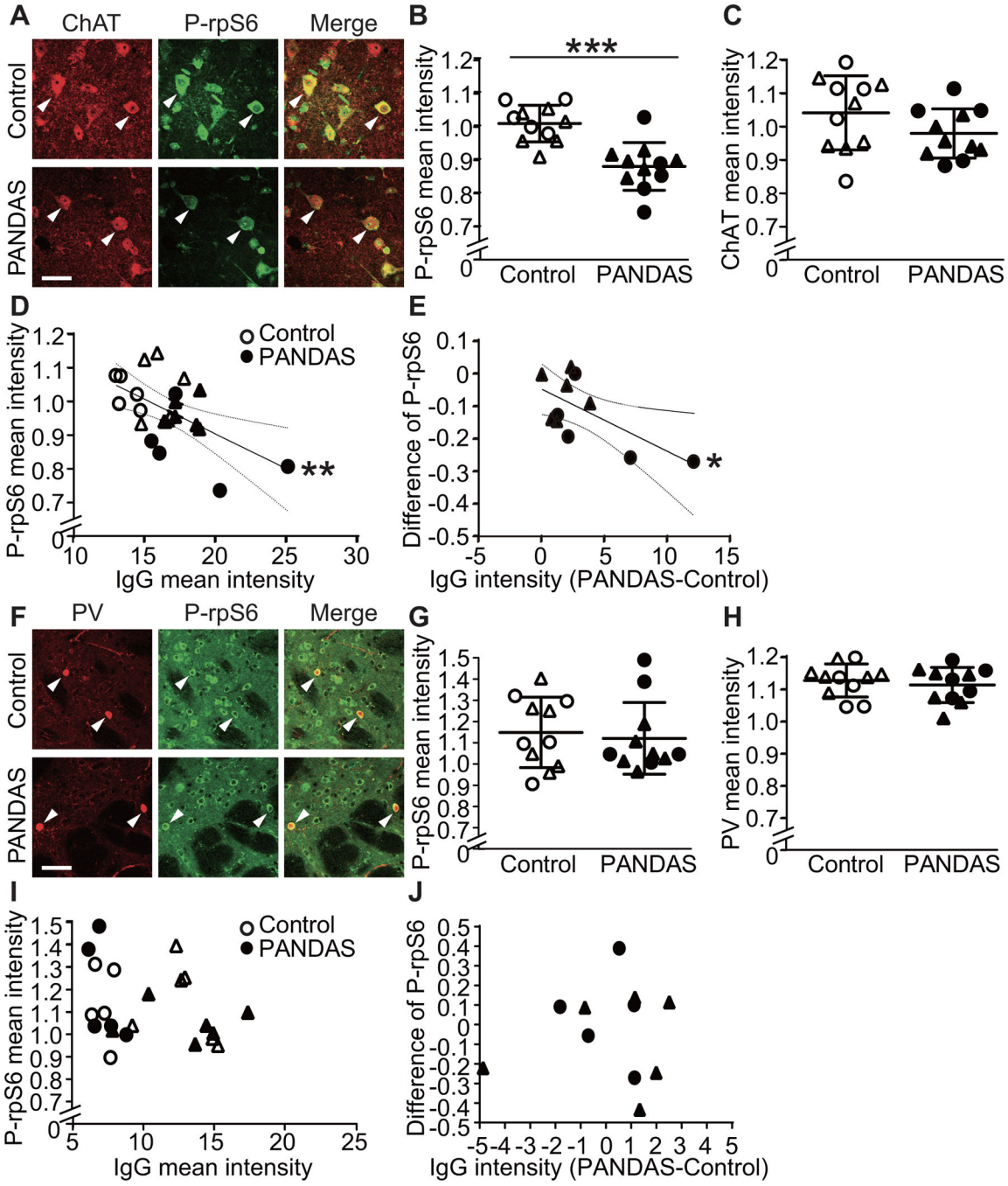

Figure 3. PANDAS serum reduces spontaneous activity in striatal cholinergic interneurons in acute mouse brains slices.

(A) Confocal images of co-staining of anti-phospho-rpS6 (green) and anti-ChAT (red) in striatal slices after PANDAS or control serum incubation. Arrowheads indicate P-rpS6/ChAT co-labeled CINs. Scale bar: 40 μm. (B) PANDAS serum incubation reduces phosphorylation levels of rpS6 in striatal CINs, relative to control serum incubation (unpaired t-test: t[20]=4.726, p=0.0001); all values are normalized to slices incubated in parallel in saline with no serum. (C) Serum incubation does not alter ChAT levels in the striatal slices. (D) Phosphorylation level of rpS6 correlates negatively with IgG binding to CINs in striatal

slices (measured separately after incubation with the same sera; see Figure 1; Pearson's correlation: r^2=0.319, p=0.006) – that is, higher IgG binding corresponds to a greater reduction in cell activity. (E) For each age- and gender-matched PANDAS-control pair, the PANDAS-control difference in IgG binding to striatal CINs correlated negatively with difference in P-rpS6 after serum incubation (r^2=0.428, p=0.029) – that is, greater differential IgG binding corresponds to greater comparative reduction in CIN P-rpS6. (F) Confocal images of co-staining of P-rpS6 (green) and PV (red) in striatal slices after serum treatment. Arrowheads indicate P-rpS6/PV co-staining. Scale bar: 40 μm. (G) PANDAS serum does not change P-rpS6 levels in striatal PV-interneurons (unpaired t-test: t[20]=0.393, p=0.7). (H) Serum incubation does not alter parvalbumin levels in the striatal slices. (I) There is no correlation between P-rpS6 levels and IgG binding to PV-interneurons in striatal slices. (J) For each age- and gender-matched PANDAS-control pair, the difference in IgG binding (PANDAS-control) to striatal PV-interneurons does not correlate with change in P-rpS6 after serum incubation. *p<0.05, **p<0.01, ***p<0.001; N=11 for each group. ●,◯ – 10 serum from the first cohort (47); ▲,△ – 12 sera from the second cohort.

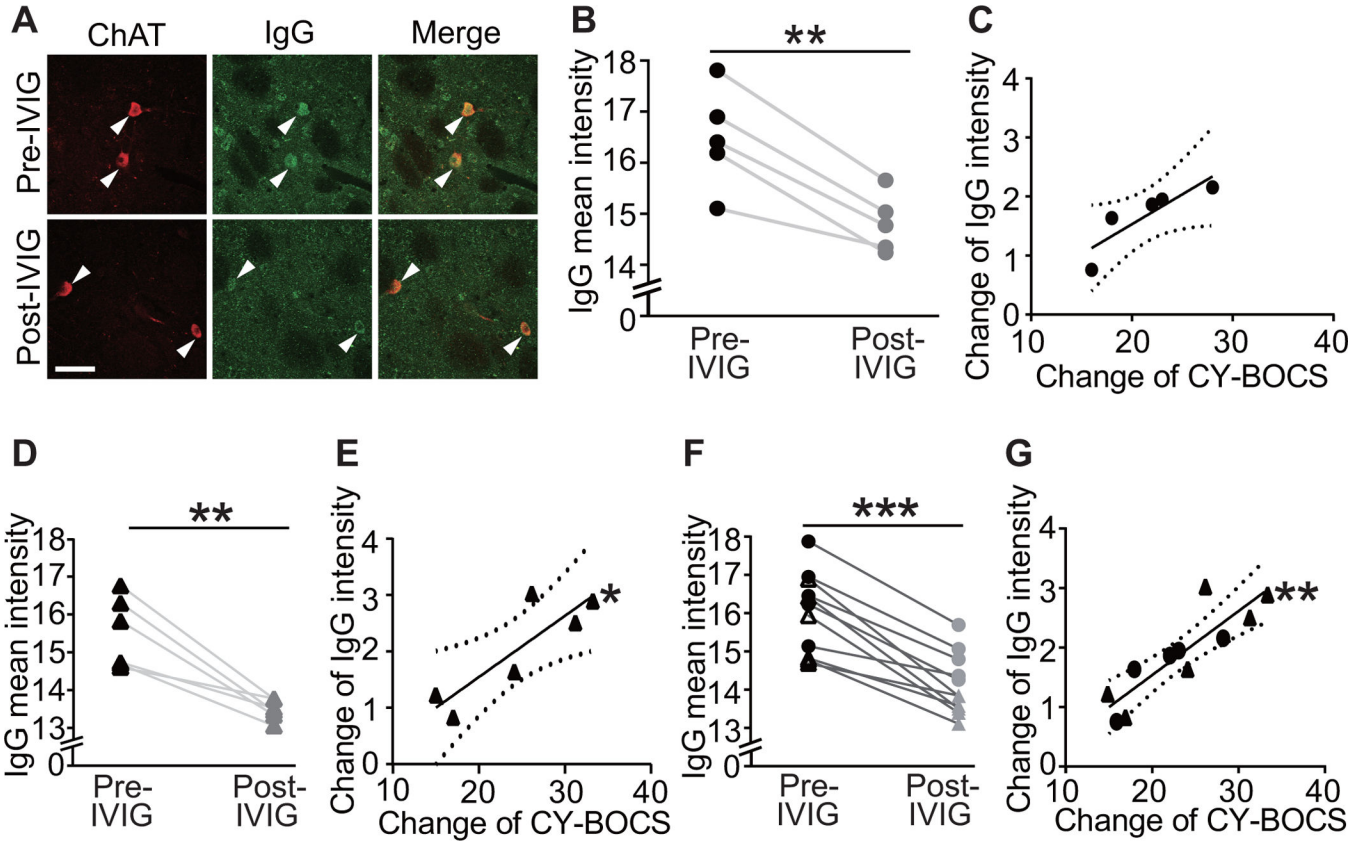

Figure 4. Reduction in PANDAS IgG binding to cholinergic interneurons correlates with decreases in CY-BOCS score following IVIG treatment.

Sera were collected at baseline (pre-IVIG) and 6–12 weeks after intravenous immunoglobulin (IVIG) treatment (post-IVIG) and tested for CIN binding. (A) Representative images of co-staining of anti-human IgG (green) and anti-ChAT (red) before and after IVIG treatment. Arrowheads indicate antibody binding to CINs. Scale bar represents 40 μm. (B) IVIG treatment results in decreased PANDAS IgG binding to CINs in the original 5 sera (paired t-test: $t[4]=6.870$, $p=0.002$); this constitutes a technical replication of our previous analysis of the same samples, using a different assay (47). (C) The change in IgG binding to striatal CINs correlated at trend level with symptom improvement (Pearson's correlation: $r^2=0.753$, $p=0.057$). (D) IVIG treatment similarly produced decreased PANDAS IgG binding to CINs in the second cohort ($t[5]=5.413$, $p=0.003$). (E) Change in IgG binding to striatal CINs correlated significantly with symptom improvement in the second cohort ($r^2=0.747$, $p=0.026$). (F) The consistent effect of IVIG treatment across the two cohorts was particularly apparent in pooled data ($t[10]=8.191$, $p<0.0001$) (G) In pooled data, the correlation between change in serum IgG binding to CINS and improvement in symptoms was particularly robust ($r^2=0.762$, $p=0.0005$). Each data point represents mean value obtained from 4–6 mice for one serum. **p<0.01, ***p<0.001; N=5 in B and C, N=6 in D and E, N=11 in F and G, for each group. Dotted lines in correlation analyses indicate 95% confidence intervals. ●,● – 5 serum pairs from the first cohort (47); ▲,▲ – 6 serum pairs from the second cohort.

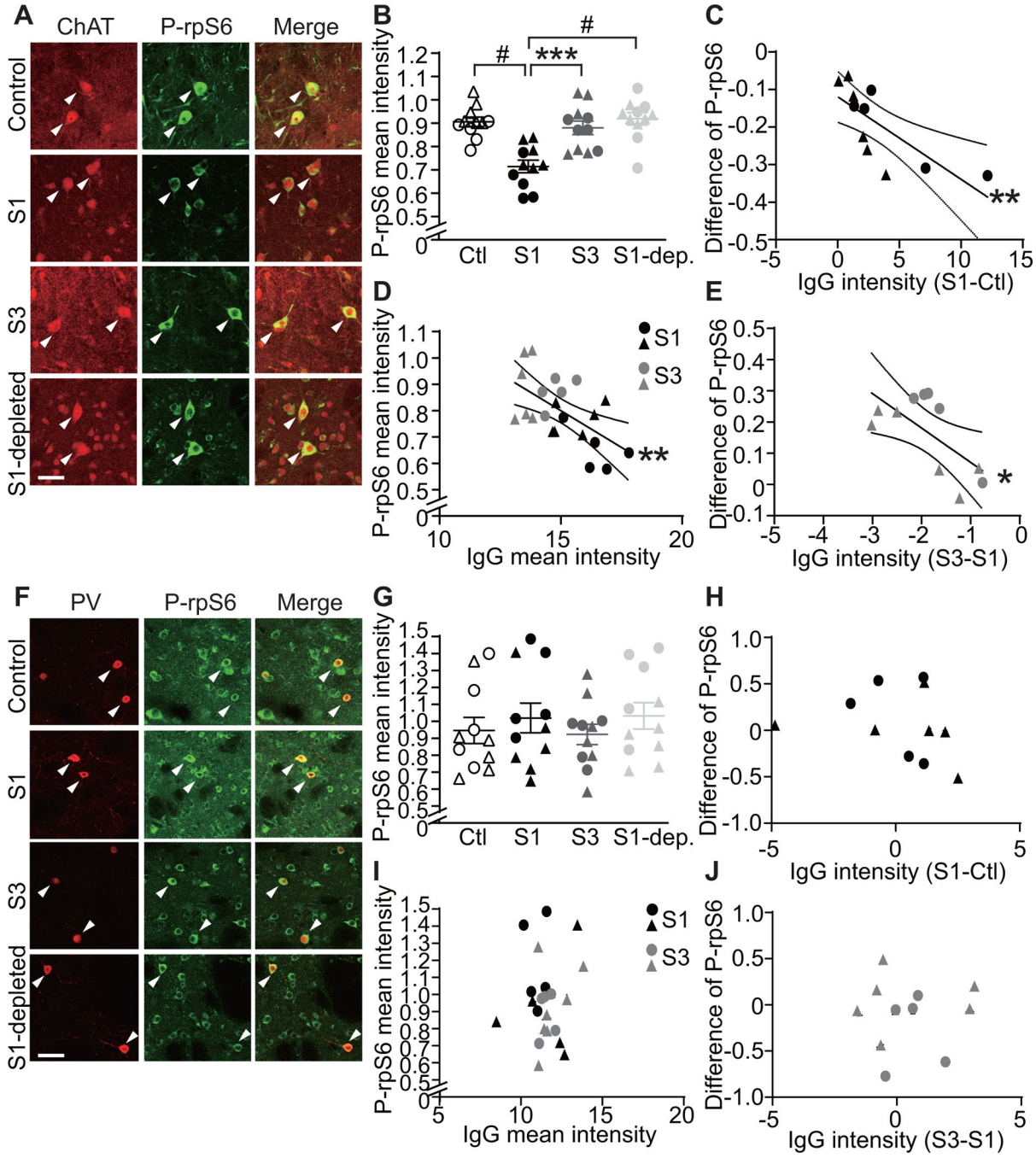

Figure 5. The ability of PANDAS serum to reduce spontaneous activity in striatal cholinergic interneurons in acute brains slices is eliminated by IgG depletion and after IVIG treatment.

Acute mouse striatal slices were treated with sera collected at baseline (S1) and 6–12 weeks after IVIG treatment (as in Figure 4; timepoint S3 in Figure S1), with IgG-depleted S1 serum (S1-dep.), or with serum from matched control subjects (Ctl). (A) Confocal images of co-staining of anti-phospho-rpS6 (green) and anti-ChAT (red). Arrowheads indicate P-rpS6/ChAT co-labeled CINs. Scale bar: 40 μm. (B) Pre-IVIG PANDAS serum (S1) reduces phosphorylation levels of rpS6 in striatal CINs compared to control, replicating Figure 3. This effect is lost in serum collected after IVIG treatment (S3) and by IgG depletion in

S1 serum (S1-dep; one-way ANOVA: F[3,40]=13.43, p<0.0001; pairwise comparisons by Tukey's post hoc test: ***p<0.001, #p<0.0001). (C) For each age- and gender-matched Pre-IVIG PANDAS-control pair, the difference (S1-Ctl) in IgG binding to striatal CINs correlated negatively with change in P-rpS6 after serum incubation (r^2=0.564, p=0.008), consistent with the results in Figure 3E. (D) In pre-IVIG (S1) and post-IVIG (S3) PANDAS serum-treated slices, P-rpS6 levels correlate with IgG binding to CINs in striatal slices, measured previously (Figure 4F; Pearson's correlation: r^2=0.346, p=0.004). (E) For each Pre-IVIG and Post-IVIG PANDAS pair, the difference (S3-S1) in IgG binding to striatal CINs (Figure 4) correlated negatively with difference (S3-S1) in P-rpS6 after serum incubation (r^2=0.440, p=0.026). (F) Confocal images of co-staining of P-rpS6 (green) and PV (red) in striatal slices after serum treatment. Arrowheads indicate P-rpS6/PV co-staining. Scale bar: 40 μm. (G) P-rpS6 levels in striatal PV-interneurons remain unchanged after serum incubation (one-way ANOVA: F[3,40]=0.497, p>0.7). (H) For each age- and gender-matched pre-IVIG PANDAS-control pair, the difference in IgG binding (S1-Ctl) to striatal PV-interneurons does not correlate with change in P-rpS6 after serum incubation (r^2=0.061, p>0.4), consistent with the results in Figure 3J. (I) In pre-IVIG (S1) and post-IVIG (S3) PANDAS serum-treated slices, P-rpS6 levels correlate with IgG binding to PV interneurons in striatal slices (r^2=0.009, p>0.6). (J) For each Pre-IVIG and Post-IVIG PANDAS pair, the difference (S3-S1) in IgG binding to striatal PV-interneurons does not correlate with change in P-rpS6 after serum incubation (r^2=0.001, p>0.9). *p<0.05, **p<0.01, ***p<0.001, #p<0.0001; N=11 for each group. ●,◯,●,● – sera from the first cohort (47); ▲,△,▲,▲ – sera from the second cohort.